



Tissue-specific analysis of lipid species in *Drosophila* during overnutrition by UHPLC-MS/MS and MALDI-MSI^S

Bryon F. Tuthill II,^{1,*} Louis A. Searcy,^{1,†} Richard A. Yost,^{2,†} and Laura Palanker Musselman^{2,*}

Department of Biological Sciences,* Binghamton University, Binghamton, NY; and Department of Chemistry,[†] University of Florida, Gainesville, FL

Abstract Diets high in calories can be used to model metabolic diseases, including obesity and its associated comorbidities, in animals. *Drosophila melanogaster* fed high-sugar diets (HSDs) exhibit complications of human obesity including hyperglycemia, hyperlipidemia, insulin resistance, cardiomyopathy, increased susceptibility to infection, and reduced longevity. We hypothesize that lipid storage in the high-sugar-fed fly's fat body (FB) reaches a maximum capacity, resulting in the accumulation of toxic lipids in other tissues or lipotoxicity. We took two approaches to characterize tissue-specific lipotoxicity. Ultra-HPLC-MS/MS and MALDI-MS imaging enabled spatial and temporal localization of lipid species in the FB, heart, and hemolymph. Substituent chain length was diet dependent, with fewer odd chain esterified FAs on HSDs in all sample types. By contrast, dietary effects on double bond content differed among organs, consistent with a model where some substituent pools are shared and others are spatially restricted. Both di- and triglycerides increased on HSDs in all sample types, similar to observations in obese humans. Interestingly, there were dramatic effects of sugar feeding on lipid ethers, which have not been previously associated with lipotoxicity. Taken together, we have identified candidate endocrine mechanisms and molecular targets that may be involved in metabolic disease and lipotoxicity.—Tuthill II, B. F., L. A. Searcy, R. A. Yost, and L. P. Musselman. Tissue-specific analysis of lipid species in *Drosophila* during overnutrition by UHPLC-MS/MS and MALDI-MSI. *J. Lipid Res.* 2020. 61: 275–290.

Supplementary key words metabolomics • matrix-assisted laser desorption/ionization-mass spectrometry imaging • lipid metabolism • ultra-high-performance liquid chromatography-tandem mass spectrometry

Drosophila melanogaster (called *Drosophila* hereafter) has become a well-established model for human disease pathophysiology due to its ease of use and high conservation with

higher organisms (1). Researchers estimate that approximately 77% of human genes involved in disease pathogenesis have a paralog in *Drosophila* (2), including those involved in obesity and its associated complications. Therefore, *Drosophila* has been used to model obesity and insulin resistance using genetic or dietary manipulations (3–6). Chronic high-sugar (HS) feeding has been shown to lead to obesity accompanied by hyperglycemia and hyperlipidemia in fly larvae and adults (5, 7). At the biochemical level, HS feeding led to a reduction in triglyceride (TG) substituent length and an increase in unsaturation in *Drosophila* larval fat body (FB) (8). Comorbidities, such as cardiomyopathy, are also observed in the fly when aged (9) and exacerbated on high-calorie diets (7, 9). Chronic overnutrition is thought to exceed the maximum capacity of adipose tissue, resulting in allostatic imbalance and lipid overflow to other tissues, including the heart and liver, or lipotoxicity [reviewed in (10, 11)]. Lipotoxicity is thought to comprise increases in a variety of lipid species, including free FAs, ceramides, diacylglycerols (abbreviated here as DGs), TGs, and acyl-carnitines, some of which have also been found in *Drosophila* diet-induced obesity models (12). The endocrine mechanisms and pathways leading to the accumulation of these putative toxins are not well understood.

Colorimetric assays for lipid quantification as well as thin-layer chromatography, gas chromatography, LC, and MS have been used to study lipid metabolism in a number of *Drosophila* paradigms [reviewed in (13)]. Metabolomic profiles correspond to altered phenotypes in a variety of

Abbreviations: DAGE, diacylglycerol ether, DG, diacylglycerol; FB, fat body; GL, glycerolipid; Glc-Cer, glycosylceramide; HS, high-sugar; HSD, high-sugar diet; Lyso-PC, lysophosphatidylcholine; Lyso-PE, lysophosphatidylethanolamine; Lyso-PI, lysophosphatidylinositol; Lyso-PL, lysophospholipid; MALDI-MSI, MALDI-MS imaging; MSI, MS imaging; OCFA, odd chain FA; PA, phosphatidic acid; PC, phosphatidylcholine; PCA, principal component analysis; PE, phosphatidylethanolamine; PI, phosphatidylinositol; PL, phospholipid; PS, phosphatidylserine; SO, sphingosine; TG, triglyceride (triacylglycerol).

¹B. F. Tuthill and L. A. Searcy contributed equally to this study.

²To whom correspondence should be addressed.

e-mail: lmusselm@binghamton.edu (L.P.M.); ryost@chem.ufl.edu (R.A.Y.)

^SThe online version of this article (available at <https://www.jlr.org>) contains a supplement.

This work was supported by Binghamton University, National Institutes of Health Grant U24DK097209, and American Heart Association Grant SDG33400207. The content is solely the responsibility of the authors and does not necessarily represent the official views of the National Institutes of Health. The authors declare that they have no conflicts of interest with the contents of this article.

Manuscript received 18 June 2019 and in revised form 12 December 2019.

Published, *JLR Papers in Press*, January 3, 2020
DOI <https://doi.org/10.1194/jlr.RA119000198>

Copyright © 2020 Tuthill et al. Published under exclusive license by The American Society for Biochemistry and Molecular Biology, Inc.

This article is available online at <http://www.jlr.org>

Drosophila genetic backgrounds and dietary paradigms (14–16). Metabolomic studies have been useful in several insect models, such as the silk worm, identifying changes in metabolite concentrations in the face of fungal infection (17). Analysis of whole mosquitos and cell culture upon infection show differential presence of metabolites (18, 19). Lipidomics, using LC-mass spectrometric methods has previously identified an array of lipids in *Drosophila* whole animal (20, 21) and tissue-specific homogenates, including lysophospholipids (Lyso-PLs), ceramides, and phospholipids (PLs) as well as other nonlipid metabolites (22). However, organ dissection in such a small organism is laborious and it is nearly impossible to analyze subregions within organs. Imaging MS techniques have gained popularity in recent years due to their ability to detect metabolites with spatial resolution within samples, including small molecules such as lipids (23) with much smaller tissue sample size. Mass spectrometric imaging has been used to measure cuticular hydrocarbons on wings and legs of the gray flesh fly, *Neobellieria bullata*, and the wings of male *Drosophila* (24). TGs and sex pheromones were also identified on the surface of whole mounted and scanned *Drosophila* adults (25). MALDI-MS imaging (MALDI-MSI) has been used to identify lipid species in mouse brains with high sensitivity (26) as well as the nematode *Caenorhabditis elegans* (27). Studies using MALDI-MSI on sectioned *Drosophila* adults have revealed localization of broad sets of compounds, including phosphatidylethanolamine (PE), phosphatidylcholine (PC), phosphatidylinositol (PI), phosphatidylglycerol, TG, phosphatidylserine (PS), and sex pheromones as well as localization of peptides and other metabolites (28). Whole mounted *Drosophila* brains have also been studied and have revealed localization patterns of different subsets of PLs within the CNS (29, 30). Although MALDI-MSI-based metabolomics has become a growing area of expertise in multiple model organisms, this tool has not extensively been used to assess lipotoxicity in obese *Drosophila*. The fly is large enough for organs to be seen, but too small for large-scale dissection and collection of tissues for traditional mass spectrometric methods. Considering the small size of *Drosophila* and the extensive genetic tools available, the development of specific quantitative MSI methods could enable increased efficiency.

Here, we use *Drosophila* to compare lipid content in organs from control and HS-fed flies. We hypothesized that lipids accumulate differentially in organs in the face of overnutrition. We used microdissection techniques to collect *Drosophila* organs for lipid analyses. MSI was used to characterize the lipidome during high-calorie feeding. By using MALDI-MSI, which gives information about lipids in individual *Drosophila* organs, we expect to find changes in lipid profiles in tissues resulting from overnutrition. We also present data using a complementary technique, UHPLC-MS/MS, which identifies a greater number of metabolites but requires a much larger number of organs. Differential accumulation of lipids in HS-fed organs could identify novel candidates for lipotoxicity. Both methods represent promising approaches to study a variety of lipids using relatively small amounts of insect tissue.

Fly lines and maintenance

All fly stocks were maintained on 5% dextrose-cornmeal-yeast-agar medium at 25°C with controlled humidity. Wild-type white-eyed *w¹¹¹⁸* flies obtained from the Vienna *Drosophila* Resource Center were used for all experiments and maintained with 12/12 h day/night light cycling. Adult flies were reared on dextrose food, then transferred to 0.15 M (5% sucrose) control diet or 1 M (34% sucrose) high-sugar diet (HSD) (5) within 24 h of eclosion, then aged for 3 or 5 weeks before euthanization for organ collection. Flies aged on the control diet were flipped onto fresh food every 2 days, whereas flies aged on HSD were flipped every 5 days in order to preserve food quality. Control diets were changed more frequently because the food consistency decreased at a quicker rate than HSD food.

Tissue collection and storage

For UHPLC-MS/MS, 100 adult hearts, 10 µl of hemolymph, and 20 FBs per replicate with equal ratio male to female organs were collected by fine dissection from flies anesthetized with Fly-Nap (trimethylamine) (31). Adult hearts and FBs were homogenized by hydraulic pressure and mechanical shearing using a 20 gauge needle and hypodermic syringe in 200 µl of PBS (pH 7.4), with 190 µl extracted for UHPLC-MS/MS and 10 µl saved for protein determination. Adult flies were impaled in the thorax using a 0.125 mm tungsten probe and placed in a 500 µl tube pierced with a 25 gauge needle and nested inside a 1.5 ml tube for hemolymph collection as described by Lung and Wolfner (32). Ten microliters of hemolymph were collected from 200 flies per replicate and centrifuged at 4°C at 2,348 *g* for 5 min. Volume was brought up to 200 µl with PBS. Adult flies for MALDI-MSI studies were anesthetized with CO₂ and then micro-dissected onto ice-cold slides. Hearts and FBs were placed on microscope slides and immediately frozen at –80°C.

UHPLC-MS/MS

Drosophila adult organs were analyzed by the South Eastern Center for Integrated Metabolomics at the University of Florida, Gainesville, FL. In short, lipids were extracted using a bacterial lipidomics extraction procedure and normalized prior to injection to the lowest sample protein concentration (33, 34). Internal standards were used to quantify lipid classes detected in both positive and negative ion modes. Two microliters of internal standards were added prior to extraction. Standards were injected with a final amount of 10 ng on the column for positive and 17 ng for negative. Lipids were quantified using the following standards: TG (15:0/15:0/15:0) for TG and diacylglycerol ether (DAGE), DG (14:0/14:0), ceramide (d18:1/17:0) for sphingolipids (SLs), PC (17:0/17:0) for PC and ether-linked PC, PE (15:0/15:0) for PE and ether-linked PE, and lysophosphatidylcholine (Lyso-PC) (17:0) for all Lyso-PL. Samples were reconstituted in 30 µl of solvent and injected via autosampler, 5 µl for negative and 3 µl for positive, into a Thermo Q-Exactive Orbitrap mass spectrometer/electrospray ionization and Dionex UHPLC and analyzed at a mass resolution of 35,000 at *m/z* 200 for both positive and negative injections. The temperature of the column was 50°C with a flow rate of 500 µl/min. To attain separation, an Acuity BEH 1.7 µm, 100 × 2.1 mm column was used with 60:40 acetonitrile:10 mM ammonium formate with 0.1% aqueous formic acid for mobile phase A and 90:8:2 2-propanol:acetonitrile:10 mM ammonium formate with 0.1% aqueous formic acid for mobile phase B. LipidMatch software was used to identify resulting peaks (35).

MSI

Organs were dissected from one fly per biological replicate, placed on a clean microscope slide and frozen at -80°C . Slides were vacuum desiccated for 1 h, washed with 150 mM of ammonium acetate, and dried for 30 min by vacuum before matrix was applied with a glass type A Meinhard nebulizer (Golden, CO) with a flow rate of 3 ml/min. The matrix consisted of 40 mg/ml 2,5-dihydroxybenzoic acid and 10 mM sodium acetate dissolved in 80:20 methanol:water. Samples were vacuum desiccated for another 15 min after matrix application to remove any remaining solvent. For both hearts and FBs, 126 ± 0.0003 mg of matrix were applied prior to MALDI imaging. Samples were analyzed in a Thermo Scientific LTQ XL linear ion trap mass spectrometer (San Jose, CA) with a MALDI ionization source consisting of a Lasertechnik Berlin MNL 106-LD N2 laser ($\lambda = 337$ nm) (Berlin, Germany). MALDI parameters included a laser energy of $6.1 \mu\text{J}$, three laser shots per spot, and a step size of $100 \mu\text{m}$ for MS and $6.1 \mu\text{J}$, three laser shots per spot with $25 \mu\text{m}$ step size for MS/MS. Ten biological replicates of each sample type were used, with three technical replicates averaged for each biological replicate. Background feature filtering was used to filter out background peaks (36) before statistical analysis using MetaboAnalyst (37). MS/MS was conducted and subsequent identification of peaks using LipidMatch (35). The fragmentation libraries in LipidMatch were edited to identify lipid species with the use of a linear ion trap mass spectrometer.

Statistical analysis

All peak area data from UHPLC-MS/MS and MALDI-MSI studies (respectively) were normalized to the total ion current. Principal component analysis (PCA), heat map, volcano plot, and ANOVA powered by MetaboAnalyst 3.0 (37) were used to estimate variation across the sample groups and a Fisher's least significant difference (LSD) was used for post hoc analysis to determine the significance between groups. Volcano plots, a univariate method, used log fold change plotted as a function of log P -value to give compounds significantly increased and decreased in presence. Fold change cut offs were set at >1.25 and <0.75 with a P -value cut off of <0.05 as identified by Student's t -test. For heat maps, Ward clustering algorithm was used to group significant compounds identified by t -test for univariate data sets and ANOVA for multivariate data sets. Heat maps show variances in fold change between biological replicates and experimental groups, whereas volcano plots indicate variances in individual compounds between experimental groups. MS/MS files were converted from .raw to .ms2 files with ProteoWizard (38). Graphs were made using GraphPad Prism software (v. 6.0).

RESULTS

Mass spectrometric analyses of *Drosophila* organs isolated from control and diet-induced obese adults

Our workflow (Fig. 1) combined MALDI-MSI and traditional UHPLC-MS/MS to characterize lipid species among tissues. In our overnutrition paradigm, we used chronic HSD feeding to induce insulin resistance, lipotoxicity, and other phenotypes reminiscent of a type 2 diabetic state, including obesity and accumulation of free FAs (5, 8, 12). Larvae were reared on 5% dextrose cornmeal-yeast-agar medium until eclosion. Adults were then transferred and aged on control (5% sucrose) or HS (34% sucrose) modified Bloomington semi-defined diets (5) for 3 weeks (MALDI-MSI) or 5 weeks for both MALDI-MSI and UHPLC-MS/MS.

Increasing dietary sucrose produces tissue-specific changes in lipid classes

First, we used traditional UHPLC-MS/MS to compare the effects of control diet and HSD in individual tissues. We analyzed mixed-sex adult w^{1118} FBs, hemolymph, and hearts at 5 weeks of age. These studies identified 383 lipids in the FB and hemolymph and 272 lipids in heart tissue. The lipids detected included species spanning glycerolipids (GLs), including TGs, DGs, monoglycerides, PLs, Lyso-PLs, SLs, ether lipids, acylcarnitines, coenzyme-Qs, and cardiolipins. A PCA scores plot was used to highlight overall variances between diets and tissues using peak areas as the variables (Fig. 2A). Each sample is shown as a single point with a 95% confidence interval ellipse representing the range of the data. Only a slight overlap in 95% confidence interval ellipses is observed between control and HS FBs, hemolymph, and hearts, indicating that a portion of the diet-dependent metabolome differed in each sample type. We were able to identify numerous specific TGs, DGs, PLs, SLs, Lyso-PLs, and ether-linked lipids (hereafter called ether lipids), all of which are classes from which at least one species was significantly differentially present between control and HS conditions (supplemental Files S1, S2, and S3). Several other lipid classes were also identified by UHPLC-MS/MS, including acyl-carnitines, cardiolipins, and coenzyme-Q8, -9, and -10. Because PCA suggested site-specific changes in a broad range of lipid compounds, we further characterized the lipidome of the FBs, hemolymph, and hearts. We focused on five overarching categories of lipid compounds: GLs, PLs, Lyso-PLs, SLs, and ether lipids. The largest confidence ellipses were repeatedly observed in the control-fed adult FBs (Fig. 2). Principal components in TGs were most dramatically affected by HS in hemolymph, while there were also apparent effects on TGs with slight overlaps in both FB and heart 95% confidence interval ellipses (Fig. 2B). Similar to TG, the greatest effects of HS on DG were in the adult hemolymph (Fig. 2C), consistent with a finding that DG plays a major role in larval hemolymph (39). By contrast, HS did not seem to affect overall PL content in any sample set despite their abundance, with overlapping ellipses in all tissues (Fig. 2D). The greatest variance in SL principal components was observed in FBs, with complete separation of 95% confidence interval ellipses. Ellipses for both control and HS heart SLs were small and overlapping, indicating that SLs varied little in this tissue (Fig. 2E). Lyso-PLs were most different in hemolymph, with no apparent effect of HS on Lyso-PL in hearts or FBs (Fig. 2F). We saw a correlation between ether lipids and dietary sugar in FBs and hemolymph with some overlap in hearts (Fig. 2G). Moving forward, we focused on the four overarching lipid classes with separation of principal components in at least one tissue: GLs, SLs, Lyso-PLs, and ether lipids.

The FB contains more saturated fat and fewer odd-numbered FA substituents when fed HS

We first assessed the lipidome of the FB, as it is the fly's primary lipid storage and metabolic tissue and is similar to the mammalian adipose and liver. As seen by PCA,

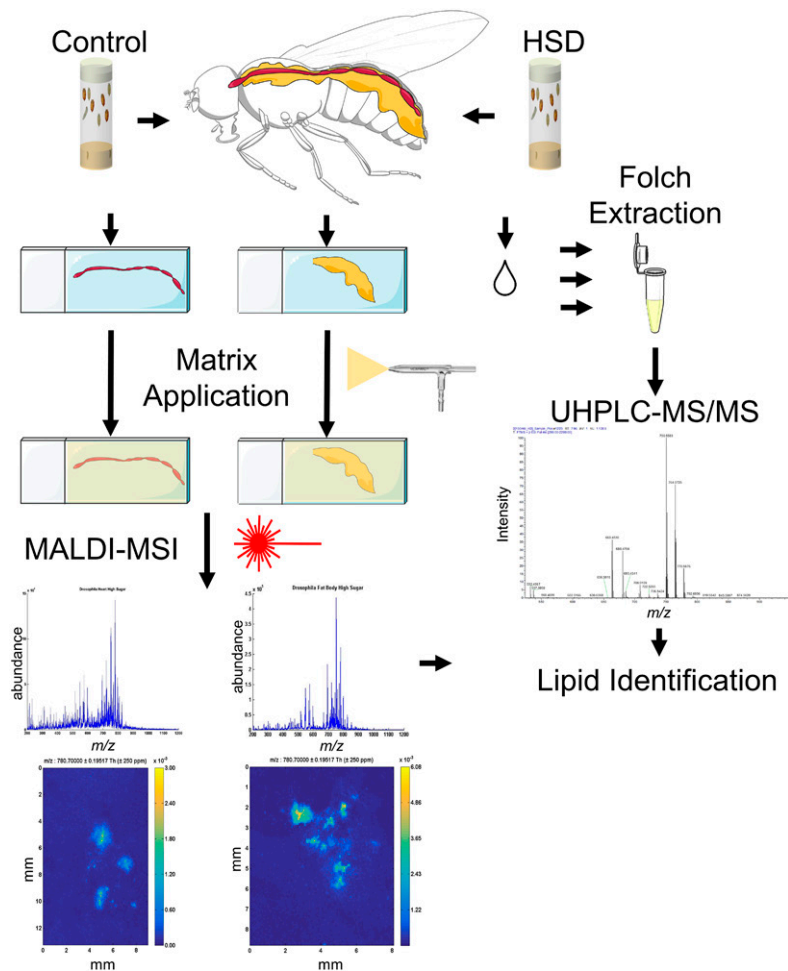


Fig. 1. Metabolomics workflow uses both UHPLC-MS/MS and MALDI-MSI for lipidomics study of over-nutrition. Adult flies were aged on control diet (0.15M sucrose) or HSD (1M sucrose). Organs were dissected and either placed on slides for MALDI-MSI or combined in tubes for analysis by UHPLC-MS/MS. For MALDI-MSI, a Meinhard nebulizer was used for matrix application. Images show the peak intensities for a specific mass range. MALDI-MSI was used to analyze multiple organs per fly. In UHPLC-MS/MS, peak heights were quantified for lipid content.

principal components of the FB lipidome varied between control and HS feeding (Fig. 3A). Each lipid was quantified relative to lipid standards added before extraction of each replicate group of 20 FBs. There were no significant changes in overall amounts of the GL, PL, SL, or other lipid classes between control and HS feeding (Fig. 3B), consistent with the PCAs in Fig. 2. GLs and PLs comprised the majority of lipids detected in FBs and were similar in abundance to each other (Fig. 3B). Total GL remained almost constant at 624.7 ng and 686.6 ng per FB between control and HS (Fig. 3B). Within the GL class, there were no overall changes in either TGs or DGs (supplemental Fig. S1A, B). PL content seemed to decrease from 1,246.8 ng to 629.9 ng per FB, although the difference was not statistically significant in FBs ($P = 0.24$, Fig. 3B). Like PLs, ether lipids trended toward a decrease, although the changes were not significant (Fig. 3B, supplemental Fig. S1C–G). Because PCAs suggested differences within classes, and quantitative MS suggested that there were few significant changes among classes, we looked at changes in subclasses within the overarching GL, SL, Lyso-PL, and ether lipid classes.

Analysis of GL pools revealed changes in the relative levels of even chain substituents and odd chain substituents as well as changes in saturation levels of both tri- and diglycerides. Even chain TGs increased ($P = 0.017$) on a

HSD, while TGs with at least one odd chain substituent decreased significantly ($P = 0.017$) (Fig. 3C). There was an overall increase in saturated and mono-unsaturated FA substituents with a corresponding decrease in relative double bond content. Even chain FAs significantly increased in saturation and mono-unsaturation ($P = 0.03$ and 0.06 , respectively), while polyunsaturation decreased ($P = 0.048$ and 0.07) (Fig. 3D). Odd chain FAs (OCFAs) exhibited an increase in saturation in FB TGs, although it was not significant ($P = 0.10$) (Fig. 3E), and a near significant decrease in substituents with two unsaturations ($P = 0.054$) (Fig. 3E). While DGs slightly increased from 0.36% to 0.6% of total GLs ($P = 0.31$) on HS (Fig. 3F), we saw a slight decrease in OCFAs substituents in DGs (Fig. 3G). Nonsignificant increases in saturated DG species were seen with nonsignificant decreases in mono- and polyunsaturated DGs (Fig. 3H), although a trend toward greater saturation was clear.

We also analyzed SLs, which include ceramides, glycosylated ceramides, sphingosines (SOs), and SMs in the FBs. There were no significant differences within these SL classes (Fig. 3I–L; supplemental Fig. S1C–E). Next, we assessed changes in Lyso-PLs and observed no differences within this class (Fig. 3M–O). Finally, we compared the relative changes in ether lipids within the FBs. There was a significant increase ($P = 0.02$) in plasmenyl-TG, also known as

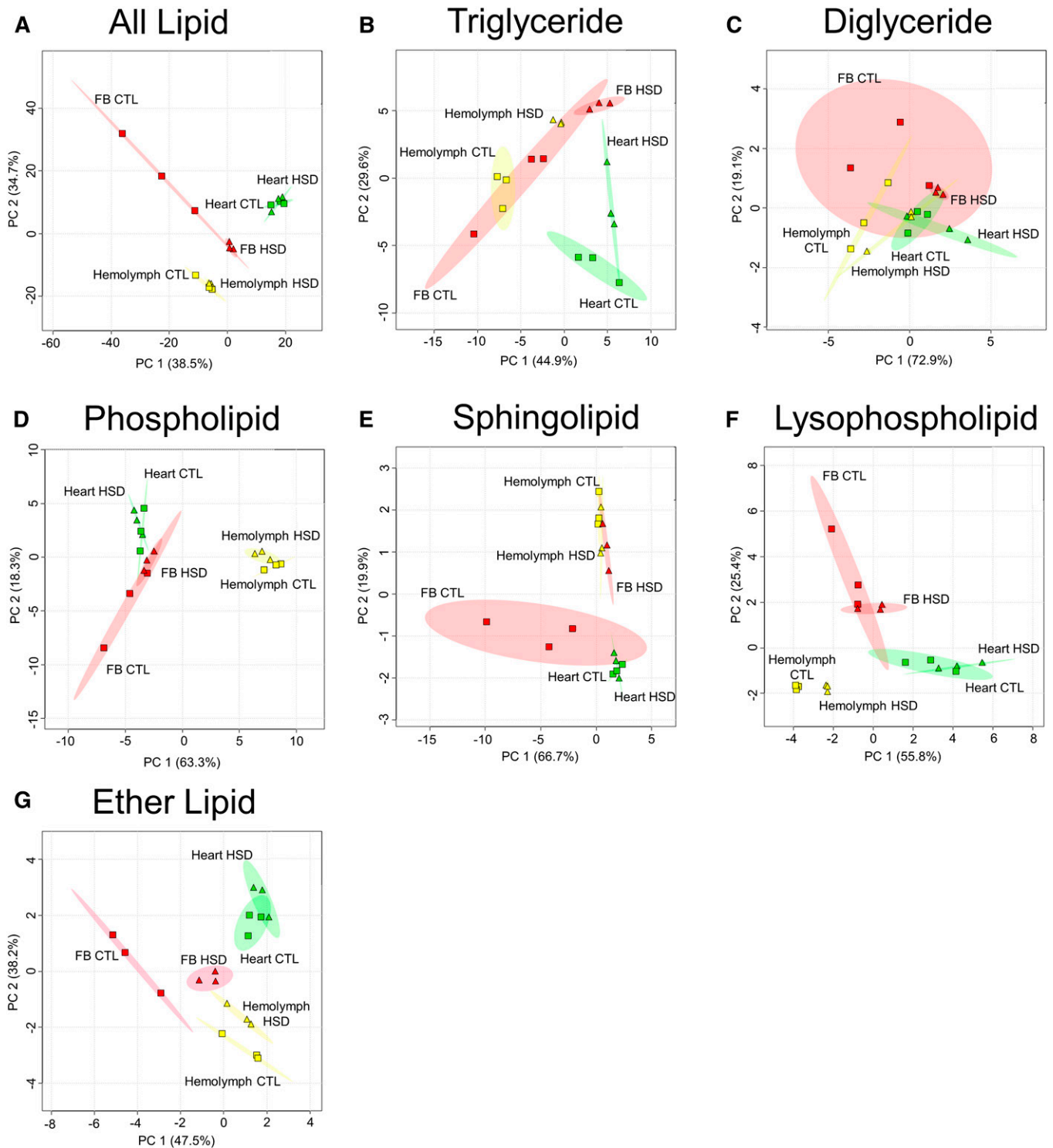


Fig. 2. HS feeding produces tissue-specific lipid profiles. A: PCA scores plot showing variances in lipid species between control (CTL) and HSD-fed FB, hemolymph, and heart at 5 weeks of age, identified by UHPLC-MS/MS. B–G: Individual PCAs of TGs (B), DGs (C), PLs (D), SLs (E), Lyso-PLs (F), and ether lipids (G) in each tissue and condition. Ellipses represent 95% confidence intervals: control diet FB, red squares; HSD FB, red triangles; control diet hemolymph, yellow squares; HSD hemolymph, yellow triangles; control diet heart, green squares; HSD heart, green triangles.

DAGEs (Fig. 3P). On a HSD, DAGEs increased from 19.3% to 64.8% ($P = 0.022$). Simultaneously, levels of plasmanyl-PC, plasmenyl-PC, and plasmanyl-PS decreased without significance (Fig. 3Q, R, U), with a significant decrease in plasmenyl-PE ($P = 0.02$) (Fig. 3T). The increase in DAGEs

with the corresponding apparent decrease in other plasmanyl and plasmenyl species indicated a shift in ether lipid metabolism that may be physiologically relevant in the HSD-fed FBs. While FB ether lipids did not change significantly when quantified relative to internal standards, the trends

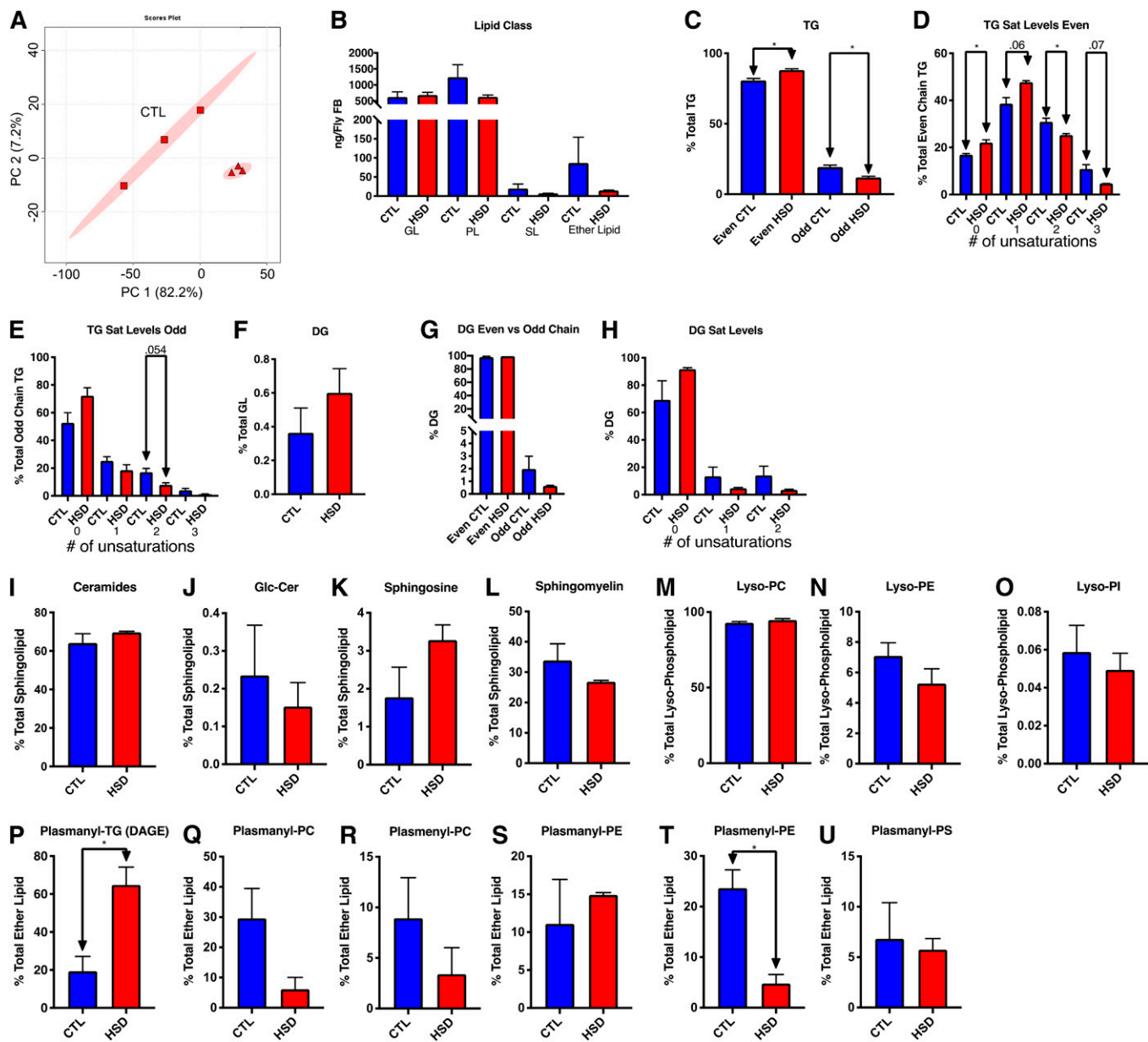


Fig. 3. FBs from adults contain more saturated fat and fewer odd-numbered FA substituents when fed HSD. A: PCA scores plot showing variances in lipid between control (CTL) and HSD-fed FBs after 5 weeks. Shown are 95% confidence ellipses. B: Quantity of each major class per FB detected in the overall lipid pool from control and HSD-fed FBs. C: Comparison of FA substituents in TGs. D: Even chain double bond content. Odd chain TGs were those with at least one odd chain substituent. E: Odd chain TG double bond content. F: DGs. G: Odd chain DG content. H: DG saturation. I: Ceramides. J: Glc-Cers. K: SO. L: SM. M: Lyso-PC. N: Lyso-PE. O: Lyso-PI. P: Plasmanyl-TG (DAGE). Q: Plasmanyl-PC. R: Plasmanyl-PC. S: Plasmanyl-PE. T: Plasmanyl-PE. U: Plasmanyl-PS. * $P < 0.05$, ** $P \leq 0.01$.

remained the same (supplemental Fig. S1F–J). More replicates and targeted MS will be used in future studies to resolve these types of interesting but low-abundance lipid species.

To get a sense of which specific lipids were diet dependent, we used both volcano plots and hierarchical clustering. A volcano plot was used to graph which lipids are both significant with a P -value of < 0.05 and a fold change of < 0.75 or > 1.25 (supplemental Fig. S2A). We identified 120 significant differentially present compounds including 57 TGs, 1 DG, 10 ceramides, 1 glycosylceramide (Glc-Cer), 3 SMs, 2 Lyso-PCs, and 14 ether lipids including two DAGE com-

pounds, which are significantly increased. There were only 10 lipids in total that significantly increased in fold change, all TGs or DAGEs, while 110 decreased. (supplemental File S1). Using hierarchical clustering, we highlighted the top 25 significant differentially present lipids with a heat map showing increases in two highly saturated medium chain-length TGs (12:0,14:0,14:1 and 14:0,14:0,16:0) and decreases in a number of longer substituent and odd chain TGs (supplemental Fig. S2B). Because we saw changes in chain composition and specific lipid classes in the FBs, we wanted to see if the same trends were present in the hemolymph.

HS feeding increased even chain and saturated FA substituents in hemolymph

As seen with FBs, principal components between control and HS hemolymph varied significantly with nonoverlapping confidence interval ellipses as depicted in PCA (Fig. 4A). Hemolymph lipids were again analyzed by class and each lipid class was quantified per microliter of hemolymph. There was a potential increase in GLs from 427.2 to 789.0 ng comparing control to HS ($P=0.10$, Fig. 4B). Unlike in FBs, PLs were much more abundant than TGs in hemolymph, and there was a significant decrease ($P=0.025$) in total PLs per microliter of hemolymph from

5,805.1 ng in control-fed flies to 4,361.1 ng per microliter of hemolymph in HS-fed flies (Fig. 4B). No changes in SLs or ether lipids were seen at the class level. Further analysis of GLs showed an HS-induced increase in even chain TGs ($P=0.009$) compared with a significant decrease in TGs with at least one odd chain ($P=0.009$), similar to trends seen in the FBs (Fig. 4C). Also, overall saturation increased with a corresponding decrease in double bond content, as seen in FBs. The abundance of saturated and mono-unsaturated even chain TGs increased significantly ($P=0.018$ and 0.002 , respectively), while polyunsaturated species with two and three double bonds both decreased significantly ($P=0.0002$

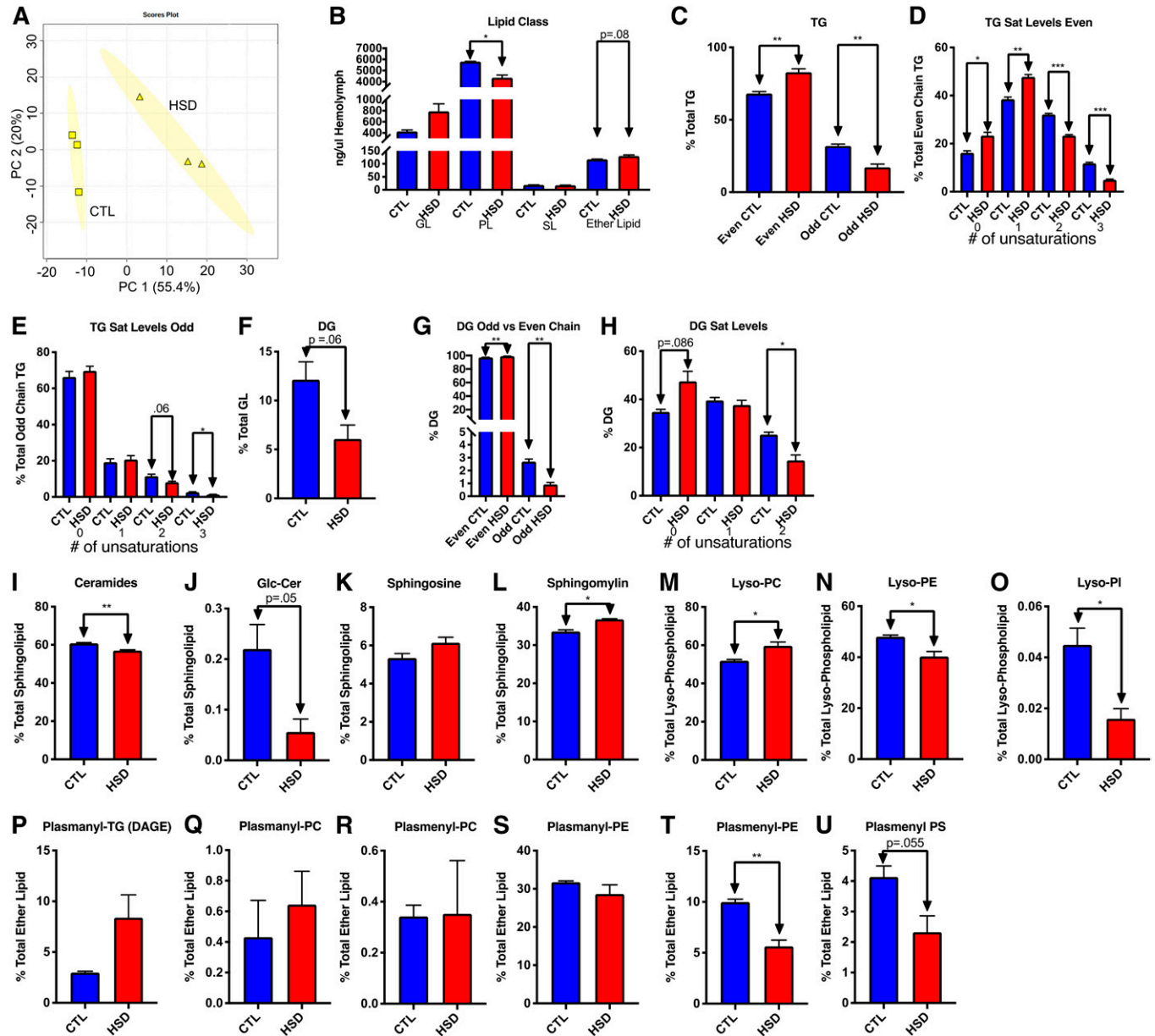


Fig. 4. As in FBs, HSD increased even chain and saturated FA substituents in hemolymph. A: PCA scores plot showing changes in lipid composition between control and HSD-fed hemolymph with 95% confidence ellipses shown. B: Quantitation of each major class in the overall lipid pool from control (CTL) and HSD hemolymph per microliter of hemolymph collected. C: Comparison of FA substituents in TGs. D: Even chain double bond content. E: Odd chain TG double bond content. F: DGs. G: Odd chain DG content. H: DG saturation. I: Ceramides. J: Glc-Cers. K: SO. L: SM. M: Lyso-PC. N: Lyso-PE. O: Lyso-PI. P: Plasmanyl-TG (DAGE). Q: Plasmanyl-PC. R: Plasmeryl-PC. S: Plasmanyl-PE. T: Plasmeryl-PE. U: Plasmeryl-PS. * $P < 0.05$, ** $P \leq 0.01$.

and 0.0004, respectively) in hemolymph (Fig. 4D), similar to results seen in the FBs. TGs with OCFA substituents followed the same trends as even chained TGs, although mostly not significant (Fig. 4E). Of the three sample types, DG concentrations were highest in hemolymph. While there was a decrease ($P = 0.06$) in DG concentration in hemolymph on HS (Fig. 4F), we did observe a higher concentration of DGs compared with FBs; 12% in control and 6% in HS hemolymph and 0.3% in control and 0.6% in HS FBs. Even chain concentration increased significantly ($P = 0.002$), while odd chain substituents also decreased significantly ($P = 0.002$) when compared with percent total DGs (Fig. 4G). Saturated DGs increased slightly with $P = 0.086$, while polyunsaturated DGs decreased significantly ($P = 0.026$) on HS (Fig. 4H). These trends of increased saturation and increased even:odd chain ratios were similar to those in the FBs (Fig. 3). Also similar to FBs, when we quantified the absolute amounts of TGs and DGs in hemolymph, we saw nonsignificant increases in TGs and decreases in DGs (supplemental Fig. S3A, B) similar to the results seen when analyzing by percent peak area.

Ceramides decreased (Fig. 4I) and SMs (Fig. 4L) increased significantly in hemolymph with P -values of 0.002 and 0.01, respectively, with no increase in SOs (Fig. 4K) and a near significant decrease ($P = 0.055$) in glycosylated ceramides (Fig. 4L). As with other lipid species, we saw similar results between relative and absolute quantities of each class (supplemental Fig. S3C–E). Lyso-PCs (Fig. 4M) increased significantly ($P = 0.046$), while lysophosphatidylethanolamines (Lyso-PEs) and lysophosphatidylinositols (Lyso-PIs) decreased significantly with P -values of 0.04 and 0.02, respectively (Fig. 4N, O). We were unable to get quantitative data on Lyso-PLs.

Like TG, ether lipid levels in hemolymph seemed to mirror changes in the FBs. While only one statistically significant change was seen (Fig. 4P–U), the trends in relative ether lipid concentrations were similar to those in FBs. There was a nearly significant 2.81-fold change in DAGEs ($P = 0.13$) (Fig. 4P) with a significant reduction in plasmenyl-PEs ($P = 0.00087$) (Fig. 4T). Quantitative data again had similar trends to relative data, with some exceptions (supplemental Fig. S3F–J).

To graphically depict the lipids that changed the most, we used a volcano plot (supplemental Fig. S4A) and found 164 significant differentially present lipids (supplemental File S2), most of which were decreased by HS feeding in the hemolymph. Overall, 33 lipids increased, while 131 lipids decreased. Among the compounds that decreased were ceramides, plasmanyl and plasmenyl-PLs, TGs, Lyso-PLs, and PLs. Interestingly, two species of DAGEs increased in abundance along with eight TGs, including the same TGs and DAGEs found in FBs (supplemental Files S1, S2). The top 25 differentially present compounds as shown by hierarchical clustering in the form of a heat map (supplemental Fig. S4B) indicated a significant decrease in TGs, ether lipids, Lyso-PLs, and one PL (PC18:1,18:1). None of the top 25 differentially present compounds were increased.

Saturated FA substituents and ether lipids may be obesity-associated lipotoxins in heart tissue

As in FBs and hemolymph, significant changes were seen in heart tissue from control to HS feeding. There were distinguishing features among principal components, as shown by nonoverlapping 95% confidence interval ellipses (Fig. 5A). We assessed changes in lipid classes by measuring total lipid content per heart (Fig. 5B). There was a compelling and nearly significant increase in GLs ($P = 0.052$) from 11.9 ng on the control diet to 31.8 ng per heart on the HSD. No change in total PLs, SLs, or ether lipids was seen after HS feeding (Fig. 5B). However, by analyzing peak area, we were again able to see distinct differences in each subclass that corresponded with trends seen with quantitative methods.

Overall, TGs made up the majority of the heart's GL pool on both diets, with TGs making up 98.3% of this pool on control diets and 96.1% on the HSD. The abundance of even chained TGs increased significantly ($P = 0.019$), while TGs with at least one odd chain substituent decreased ($P = 0.019$) (Fig. 5C). Saturated and mono-unsaturated TGs increased without significance, while TGs with polyunsaturated FA substituents decreased significantly ($P = 0.003$ and 0.006) (Fig. 5D) consistent with trends seen in FB and hemolymph lipid pools. Interestingly, saturation levels in TGs with an odd chain remained unchanged by HS (Fig. 5E), which was not the case in hemolymph or FBs. The relative proportion of DGs increased without significance (Fig. 5F) from 1.7% of GLs on the control diet to 3.9% on the HSD. Cardiac even chain DGs increased significantly ($P = 0.003$) and odd chain DGs decreased significantly ($P = 0.003$) (Fig. 5G) as observed in FB TG substituents. In contrast with DGs in FBs or hemolymph, which often contained unsaturated FAs, almost all DGs (>98%) in the heart consisted entirely of saturated FA substituents. (Fig. 5H). To confirm peak area approximated lipid concentration, we again compared select lipid classes by mass. There were 523% and 187% increases in TGs and DGs in HSD-reared hearts (supplemental Fig. S5A, B), although these were not significant ($P = 0.083$ and 0.085, respectively). There were no changes in ceramide, glycosylated ceramide, SO, SM, Lyso-PC, or Lyso-PE as a proportion of each class (Fig. 5I–M) or in absolute quantities (supplemental Fig. S5C, D). Lyso-PI and plasmanyl-PS were not detected in heart tissue. Commensurate with findings in both FBs and hemolymph, we saw a relative increase in DAGE ($P = 0.011$) (Fig. 5O) with a corresponding decrease in plasmanyl- and plasmenyl-PE ($P = 0.0062$ and 0.0033, respectively) (Fig. 5R, S), indicating a possible shunt from plasmanyl- and plasmenyl-PL production to plasmanyl-TG production. No significant changes were seen in ether lipids when quantified, although the trends were once again consistent (supplemental Fig. S5E–H). A volcano plot (supplemental Fig. S6A) showed 44 significant differentially present and significant compounds with a $P < 0.05$ and a fold change < 0.75 or > 1.25 . A heat map of the top 25 differentially present compounds found in the heart showed significant increases in DAGEs as well as several odd chain TGs with a single SO, glycosylated ceramide, DG, and Lyso-PC decrease (supplemental Fig. S6B). Twelve lipids decreased in abundance in hearts after

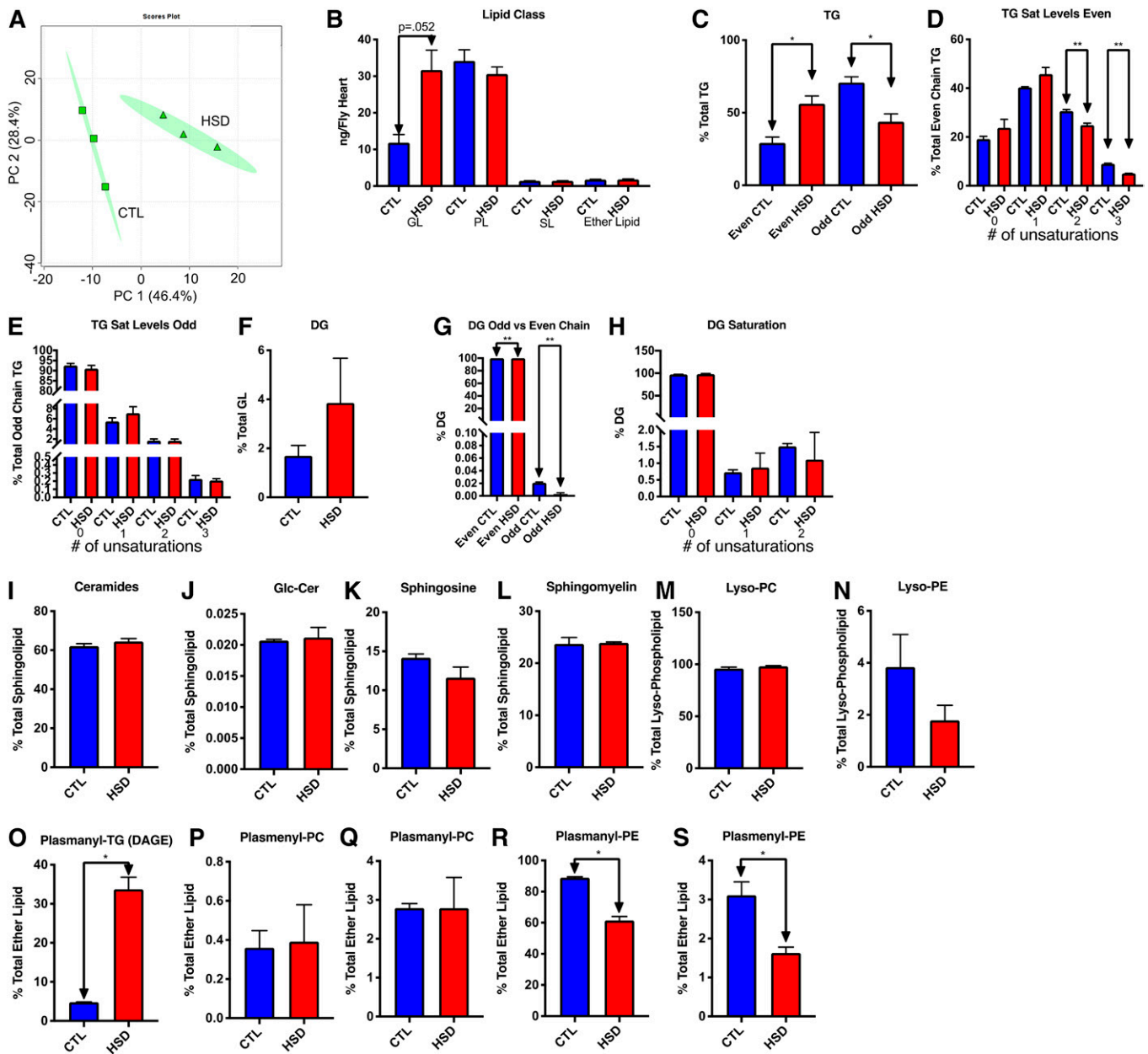


Fig. 5. Saturated FA substituents and plasmalogens may be obesity-associated lipotoxins in heart tissue. A: PCA scores plot showing changes in lipid composition between control (CTL) and HSD-fed hearts with 95% confidence ellipses shown. B: Quantity of each class in the overall lipid pool from control and HSD fed hearts. C: Comparison of FA substituents in TGs. D: Even chain double bond content. E: Odd chain TG double bond content. F: DGs. G: Odd chain DG content. H: DG saturation. I: Ceramides. J: Glc-Cers. K: SO. L: SM. M: Lyso-PC. N: Lyso-PE. O: Plasmanyl-TG (DAGE). P: Plasmanyl-PC. Q: Plasmanyl-PC. R: Plasmanyl-PE. S: Plasmanyl-PE. Lyso-PI and plasmanyl-PS were not observed in fly hearts. * $P < 0.05$, ** $P \leq 0.01$.

HS feeding, including PLs, SLs, Lyso-PLs, and a DG, while 32 lipids increased, including 25 TGs and seven DAGEs (supplemental File S3). Because we saw differences in the fly lipidome using UHPLC-MS/MS, we sought to confirm and extend our findings using MALDI-MSI, which requires less tissue and can provide spatial information about metabolite abundance.

MALDI-MSI reveals temporal and diet-dependent changes in lipid content

MSI is a technique that shows the spatial distribution of molecules within a mass spectrometric analysis. Although

UHPLC-MS/MS is able to identify many specific lipids, a large number of flies and person-hours are required. MALDI-MSI offers visualization of molecular intensity across a sample and the benefit of mass spectra from individual fly organs (27). Therefore, we developed a MALDI-MSI approach to analyze the lipidome of organs from flies fed control or HS diets.

MSI was used to complement traditional MS for the analysis of our tissue-specific HSD feeding paradigm. Matrix application is performed with a Meinhard nebulizer, and then position-specific mass spectra are acquired by a MALDI ionization source and are used to generate MS

images. Each image shows the peak intensities for a specific mass range. Multiple organs were analyzed with MALDI-MSI and then separated into individual peak lists by averaging the mass spectra over each organ. This approach was able to detect peaks in organs from flies fed either control diet or HSD for 3 weeks. The sample images shown in Fig. 1 represented the distribution of PC (36:4) in heart on the left and FB on the right. The peak for PC (36:4) spans the mass range from 782.2 to 783.2 and was normalized to the signal from the total ion chromatogram (Fig. 1). The image of PC (36:4) defined the tissue boundaries of samples from which all biologically relevant signals will be localized. A mass range of m/z 200–2,000 was used during MALDI-MSI experiments. Peak height and m/z ratios were used to compare samples consisting of FBs or hearts. Studies using MALDI-MSI resulted in tentative identifications of a number of different lipids. Ten individual phosphatidic acids (PAs), which were not identified in UHPLC-MS/MS, were also identified by class.

Mass spectrometric imaging was performed on each organ, with three technical replicates averaged together from each of the 10 biological replicates of each organ. Mass spectra were acquired over an area containing 10 biological replicates of a specific organ with a 100 μm^2 step size. One biological sample is represented by the average of all the spectra within the boundaries of that sample. Data were analyzed using MetaboAnalyst to create volcano plots, heat maps, and PCA scores plots with 95% confidence interval ellipses. For PCAs, we used the complete feature list to understand trends in diet-dependent lipid accumulation, while volcano plots and 3–5 week PCA comparisons incorporated LipidMatch to tentatively identify lipids from the MS/MS data. A PCA was first conducted, comparing FBs from control and HS-fed flies at 3 and 5 weeks (Fig. 6A, B) using MALDI-MSI feature lists including 733 features found in 3 week FBs and 417 detected at five weeks by m/z . As seen by separation of 95% confidence intervals, increased variation comparing HS-fed adult FBs to those from control-fed flies is shown by the principal components, suggesting that at both time points FB lipid content varies between diets. Using LipidMatch, we were able to tentatively identify 72 peaks in 3 week FBs and 55 in 5 week FBs. Of those, 56 lipid identities were determined by MS/MS with tail-specific fragments, and 16 lipids were identified with class-specific fragmentation in 3 week FBs, while 42 peaks identified multiple isobaric lipids by compound and 13 by class in 5 week FBs. A volcano plot was used to identify significant compounds that were increased or decreased in fold change. We found 45 significant differentially present features at 3 weeks (supplemental File S4) (Fig. 6C) and 23 at 5 weeks (supplemental File S5) (Fig. 6D). There were eight features differentially present at both time points, some of which differed in the direction of relative change. Of these eight compounds, we noted HS-induced increases in monogalactosyldiacylglycerol, PA, and oxidized PL, with decreases in PCs and TGs at 5 weeks, whereas at 3 weeks all species decreased.

Because there seemed to be a temporal difference in differentially present lipids, we compared lipid profiles between 3 and 5 weeks on control diets (Fig. 6E) and HSDs (Fig. 6F). Analyses of principal components between 3 and 5 week FBs on control diets and HSDs indicated variance, as noted by separation shown in PCA plots (Fig. 6E, F). When 3 and 5 week FBs from control diets were compared, we saw 27 differentially present features representing multiple lipid isoforms (supplemental File S6). When 3 and 5 week HSD FBs were compared, 35 differentially present features were identified (supplemental File S7). Taken together, these studies suggest that the FB lipidome changes as a function of diet and time.

In addition to FBs, we compared changes in the heart lipidome as a function of diet and time. Cardiac MALDI-MSI data included 727 features found at both 3 and 5 weeks by m/z . PCAs showed little change in principal components between control diets and HSDs, as seen by overlapping 95% confidence interval ellipses (Fig. 7A) at 3 weeks. At 5 weeks, control and HS heart lipid PCA ellipses diverge, indicating increased effects of HS on the heart lipidome compared with 3 weeks of HS feeding (Fig. 7B). LipidMatch identified 147 peak features by compound and 38 peak features by class, including PA, which was not identified by UHPLC-MS/MS in our heart samples. Volcano plots highlighted 38 significant differentially present identified features that were HS-dependent at 3 weeks of age (Fig. 7C) and 70 at 5 weeks (Fig. 7D) consistent with the increased divergence of PCA ellipses at 5 weeks. The HSD led to increases in TGs, ether lipids, and oxidized PLs with decreases in numerous PA species noted at both time points (supplemental Files S8, S9). Nineteen features were affected by HS feeding at both time points (supplemental Files S8, S9). Of the 19 features, we noted decreases in 12 and increases in 7. Interestingly, highly saturated lipids, including PC 16:0/16:0, TG 12:0/14:0/16:0, and TG 12:0/14:0/16:1 (supplemental Files S8, S9), had an increase in fold change at both time points, with 5 weeks being increased from 3 weeks. The TGs were also found to increase in HS-fed fly hearts at 5 weeks in UHPLC-MS/MS (supplemental File S3).

This increase in the number of significantly different lipids after 5 weeks of HS feeding could indicate a temporal change in lipid accumulation. When identified features from 3 and 5 week hearts on both diets were compared by PCA, we saw substantial overlaps between time points (Fig. 7E, F). Control diets from 3 and 5 week hearts were compared; this revealed 80 differentially present features (supplemental File S10), whereas only 7 features differed significantly between 3 and 5 week HS-fed fly hearts (supplemental File S11). In MALDI-MSI, we noted a nearly significant decrease in mono-unsaturated PA ($P = 0.09$) and a significant increase in PA with two unsaturations ($P = 0.012$) between hearts at 3 and 5 weeks on a HSD, even though no significant change was observed in total PA in heart between ages (supplemental Fig. S7; supplemental Files S8, S9). Therefore, both diet and time had an effect on the heart lipidome.

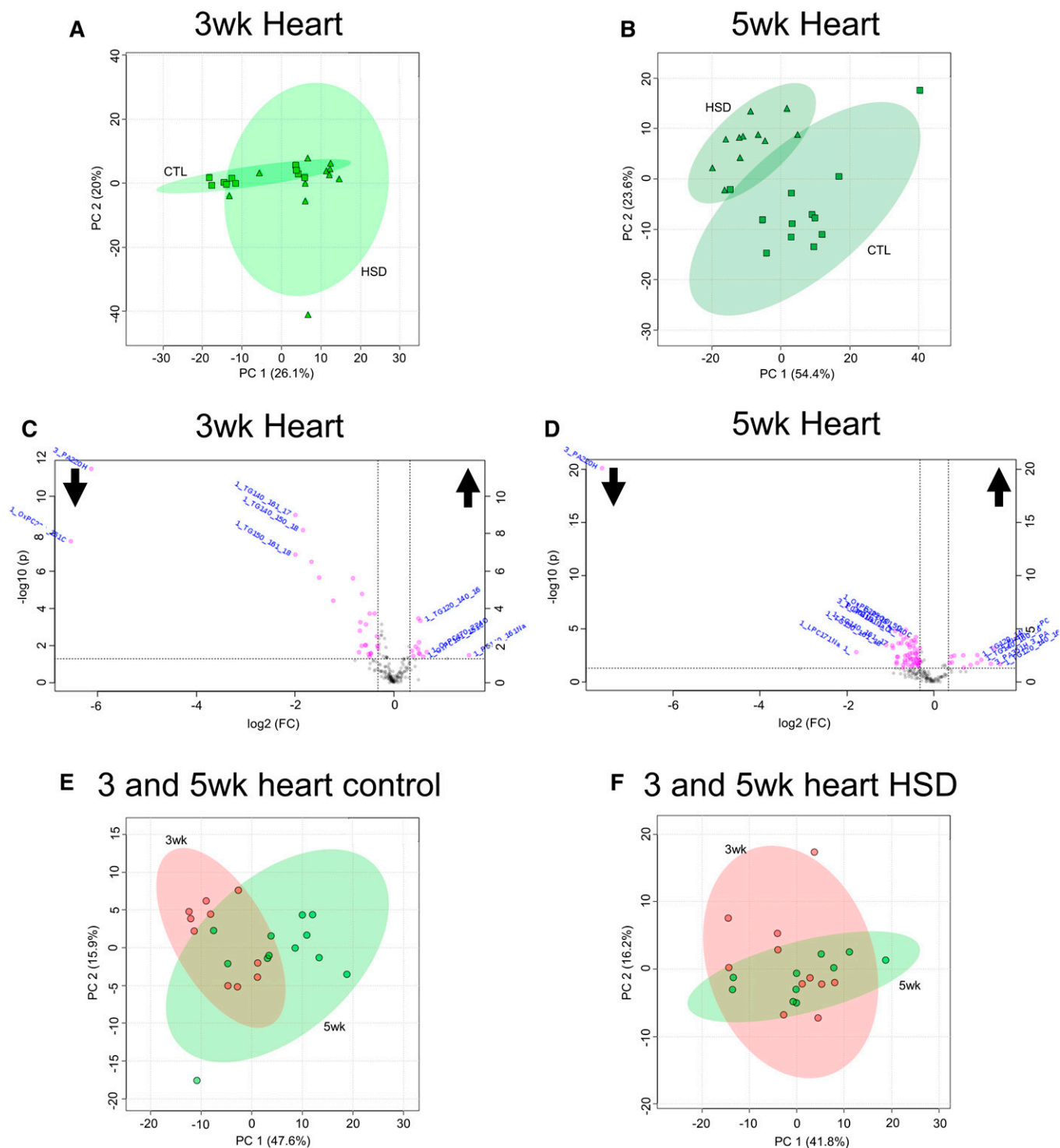


Fig. 7. HSD feeding produces significant differences in the heart lipidome, compared with control (CTL) feeding. PCAs generated for 3- and 5-week-old fly hearts on control diet and HSD (A and B, respectively) with accompanying volcano plots showing significant and differentially present identified features identified by MALDI-MSI and LipidMatch (C, D). PCAs comparing 3 and 5 week control hearts and 3 and 5 week HSD hearts (E and F, respectively). Cutoffs of 0.75- and 1.25-fold change and 0.05 *P*-value were used for volcano plots.

endocrine or cellular processes by which lipids overload and exit typical storage tissues, such as the adipose tissue in mammalian species or the FB in *Drosophila*. This study showed increases in lipid content in our HS model of caloric overload and possible lipotoxicity that was tissue and diet dependent. Overall, the most variability was seen in the FB (Fig. 2), as measured by the size of the confidence

interval ellipses in PCA score plots. This is consistent with the FB's role as a dynamic lipid storage depot similar to the mammalian liver and adipose [reviewed in (42)]. As in previous fly and mammalian studies, TGs were the major class of lipids that were affected by overnutrition.

Across all sample types, we observed a relative increase in even chain FA content and a reduction in OCFA content

on HSDs. This phenomenon could be due to a diet-dependent change in gut microbiota. Enteric bacteria are known to make odd chain FAs (43), so reduced lipogenesis by the gut microbiome is consistent with the observed shift from odd to even. One study showed that the HSD seemed to lead to an overall reduction in the size of the microbiome (44). Antibiotic feeding had bigger effects on control compared with very small effects on HS-fed flies (45), consistent with a model where the gut microbiome is smaller or less physiologically relevant under HS feeding conditions. A recent study of *Drosophila* and the parasitic microbe *Wolbachia* showed that OCFAs are strongly associated with the presence of the bacterium (46). Taken together, we hypothesize that the gut microbiota contributes a portion of OCFAs and HS reduces OCFAs via changes in the gut commensal population. This model is consistent with research from the Douglas laboratory, which showed that the effects of commensals on metabolite concentrations differed between control and high glucose diets (47).

In order to consider the potential origin of hemolymph and heart lipids, we compared them to the FB. We noted that the relative double bond content of FA substituents changed in an organ-specific and lipid-specific manner. FB and hemolymph double bond content in GLs decreased overall with fewer polyunsaturated and more saturated or monounsaturated species. Heart double bond content in DGs was unusually low compared with FB and hemolymph and heart TGs had more OCFAs compared with other sample types, indicating that heart lipids may be derived from a different pool than FB and hemolymph lipids. Interestingly, while most DGs were saturated in heart, most TGs were not, suggesting that the third substituent may arise from a different FA pool than the first two.

Lipotoxicity is observed in diseases including metabolic syndrome, obesity, cardiovascular disease, nonalcoholic fatty liver disease, and T2D. High concentrations of several lipids are thought to be toxic and contribute to the onset of comorbidities associated with adipose, heart, and liver dysfunction in these metabolic diseases. Potential lipotoxins include DGs, ceramides, nonesterified FAs, acyl-carnitines and VLDLs [reviewed in (10, 11, 48, 49)]. Although free FAs and lipoproteins were not analyzed in the current study, one possible lipotoxin is the saturated free FA palmitate, which is sufficient to induce lipotoxicity in cultured cardiomyocytes (50) and hepatocytes (51) as well as in animal models (52). Several of lipids that were increased by HS feeding contained palmitate as a substituent. In many studies, palmitate produces more severe phenotypes than the unsaturated FA oleate, including studies in cultured human cardiomyocytes (53). Saturated FA substituents are thought to have increased toxicity in both free and esterified forms. We saw increases in saturated FA substituents in both DGs and TGs (Figs. 3D, 4D, H). Di-saturated GLs such as DGs have been shown to be strongly correlated with lipotoxicity in cultured human cells when supplemented with excess palmitate (54), and reducing DG, improves insulin resistance and function of the rodent heart (55). Dietary saturated FAs are associated with in-

creases in intrahepatic TG, in patients suffering from non-alcoholic fatty liver disease (56) and serum LDL cholesterol (57).


Ceramides increase apoptosis; reducing ceramides improves insulin resistance in rodents (58, 59). Interestingly, in mice, increasing ceramide saturation led to improved lipid homeostasis (60), so there is a complex relationship between FA saturation and pathophysiology. These two established markers for lipotoxicity, DGs and ceramides, both increased in FBs and hearts after HS feeding but did not reach statistical significance. Previous studies in *Drosophila* linked increased ceramide accumulation to lipotoxicity in heart and muscle (61, 62). Slight but insignificant increases in overall ceramides in the fly heart and FB by UHPLC-MS/MS were observed in our HS model of overnutrition. Interestingly, the majority of ceramides detected in our 5-week-old fly hearts (99.7%) were monounsaturated with (0.3%) polyunsaturated species. We saw HS-induced increases in hemolymph Cer17:1/14:0 and Cer17:1/16:1, indicating that specific ceramides may play a role in cardiac pathophysiology associated with overnutrition. Because ceramides and DGs are found at lower abundance than TGs, quantification is challenging, especially with small sample sizes. Future studies may be able to use targeted metabolomics or thin-layer chromatography to separate lipids before UHPLC-MS/MS and increased biological replicates for more detailed studies of ceramides and DGs, which may help to determine whether specific DGs or ceramides play conserved roles in *Drosophila* HS-induced lipotoxicity.

Ether lipids are an interesting class of potential lipotoxins that arose from our study. Little is known about ether lipids in humans, with the bulk of research having been conducted on aquatic taxa (63). It has been postulated that ether lipids are scavenger molecules and protective against biochemical damage [reviewed in (64)]. Ether lipids are thought to be made in peroxisomes, which are associated with diabetes and other peroxisomal biogenesis disorders [reviewed in (65, 66)]. PPAR- γ , a transcription factor that regulates lipid metabolism in T2D, is activated by ether lipids downstream of FA synthase activity in 3T3-L1 adipocytes (67). Diabetic *ob/ob* mice with disruption of PPAR- γ 2 display increased severity of disease accompanied by decreases in plasmalogen species in multiple tissues, including adipose tissue (68). Diabetic patients also have decreased serum ether-linked PEs (69) and increases in ether-linked PCs in serum of diabetic patients (70). This is commensurate with our findings where we see decreases in overall plasmalogen-PE in all tissues as well as a slight but insignificant increase in overall ether-linked PCs in fly hemolymph. FA synthase deficiency has been shown to cause lipotoxic defects in mouse neutrophils along with decreased ether-linked PLs and increased ceramide (71). Both UHPLC-MS/MS and MALDI-MSI identified numerous ether lipids in all tissues at all time points in our studies; however, the species identified by each were different, showing the power of using both methods in conjunction. There was a shift in all sample types from ether-linked PL to DAGE species, indicating that DAGEs may serve as HS-induced lipotoxins in our model. In agreement with this, a

similar compensatory change between DAGEs and ether-linked PLs has been seen in aged mice (72).

It will be interesting to test which lipotoxins function analogously between *Mammalia* and the fly. Relative increases in DGs and TGs in HS-fed flies corresponded to previous observations in obese rodents and humans. Numerous clinical studies on metabolic syndrome and T2D show increases in obesity as well as cardiac and serum TGs and DGs (40, 69). High-fat diets in rats have been shown to increase hepatic TG and fatty acyl-CoA (73). Other changes in flies were also reminiscent of the mammalian lipidome during overnutrition. Obese, type 2 diabetic mice fed a high-fat diet displayed a decrease in Lyso-PC 18:1 and an increase in even chain TGs in plasma (74). Commensurate with these findings, we observed a decrease in Lyso-PC 18:1 and an increase in even chained TGs of varying chain length in hemolymph. In diabetic patients, serum Lyso-PL and plasmenyl-PC were negatively correlated with diabetes (40). Here, in a fly model of T2D, we saw similar results, with decreases in plasmenyl-PC and Lyso-PL species.

Significant changes in several lipid classes were also observed in the fly heart and FB using PCAs generated from MALDI-MSI spectra. *Drosophila* adults have been analyzed by MALDI-MSI and shown to have differential presence and localization patterns of seven distinct lipid classes in cryo-sections, including TGs and PLs (75). While the effects of diet on the tissue-specific fly lipidome have previously been reported (76, 77), MALDI-MSI has yet to be used in this context, and to our knowledge, MALDI-MSI has not previously been used to analyze the fly heart. Recently, MALDI-MSI was used to identify PL and PL precursor species after myocardial infarction in rat hearts (78). We were surprised to see so much overlap between control and HS MALDI-MSI heart spectra at time points when HS feeding impairs heart function (7). One possible explanation for this is that because the heart is a nontypical storage tissue and is made of a variety of cell types, variation in the lipidome between regions of the heart is to be expected. In other studies in the fly brain, lipids including PE, TG, DG, and PC were found to be spatially distributed (30). Using MALDI-MSI, we saw increased double bond content in the DG precursor PA, which also contributes to PL and ether lipid biosynthesis in aged flies. Future studies could include the use of MALDI-MSI to localize additional lipids of interest that accumulate within distinct regions of the FB, digestive tract, CNS, or heart after overnutrition. The locations in which we detect these compounds are likely to provide clues about their function and effect on pathophysiology.

Ultimately, our goal is to deduce the biochemical and molecular genetic mechanisms that contribute to diet-induced lipotoxicity and metabolic disease using this fly paradigm. This work has potential applications in other insect taxa as well as a range of small model systems. 

The authors would like to thank the University of Florida's Southeast Center for use of the Integrated Metabolomics core facility, especially Dr. Timothy J. Garrett and Joy Guingab. The authors also thank Ty Whitbeck for preparing *Drosophila* organ

illustrations and the Vienna *Drosophila* Resource Center for fly stocks.

REFERENCES

1. Pandey, U. B., and C. D. Nichols. 2011. Human disease models in *Drosophila melanogaster* and the role of the fly in therapeutic drug discovery. *Pharmacol. Rev.* **63**: 411–436.
2. Reiter, L. T. 2001. A systematic analysis of human disease-associated gene sequences in *Drosophila melanogaster*. *Genome Res.* **11**: 1114–1125.
3. Böhni, R., J. Riesgo-Escovar, S. Oldham, W. Brogiolo, H. Stocker, B. F. Andruss, K. Beckingham, and E. Hafen. 1999. Autonomous control of cell and organ size by CHICO, a *Drosophila* homolog of vertebrate IRS1-4. *Cell.* **97**: 865–875.
4. Grönke, S., A. Mildner, S. Fellert, N. Tennagels, S. Petry, G. Müller, H. Jäckle, and R. P. Kühnlein. 2005. Brummer lipase is an evolutionary conserved fat storage regulator in *Drosophila*. *Cell Metab.* **1**: 323–330.
5. Musselman, L. P., J. L. Fink, K. Narzinski, P. V. Ramachandran, S. Sukumar Hathiramani, R. L. Cagan, and T. J. Baranski. 2011. A high-sugar diet produces obesity and insulin resistance in wild-type *Drosophila*. *Dis. Model. Mech.* **4**: 842–849.
6. Pasco, M. Y., and P. Léopold. 2012. High sugar-induced insulin resistance in *Drosophila* relies on the lipocalin neural Lazarillo. *PLoS One.* **7**: e36583.
7. Na, J., L. P. Musselman, J. Pendse, T. J. Baranski, R. Bodmer, K. Ocorr, and R. Cagan. 2013. A *Drosophila* model of high sugar diet-induced cardiomyopathy. *PLoS Genet.* **9**: e1003175.
8. Musselman, L. P., J. L. Fink, P. V. Ramachandran, B. W. Patterson, A. L. Okunade, E. Maier, M. R. Brent, J. Turk, and T. J. Baranski. 2013. Role of fat body lipogenesis in protection against the effects of caloric overload in *Drosophila*. *J. Biol. Chem.* **288**: 8028–8042.
9. Birse, R. T., J. Choi, K. Reardon, J. Rodriguez, S. Graham, S. Diop, K. Ocorr, R. Bodmer, and S. Oldham. 2010. High-fat-diet-induced obesity and heart dysfunction are regulated by the TOR pathway in *Drosophila*. *Cell Metab.* **12**: 533–544.
10. Birse, R. T., and R. Bodmer. 2011. Lipotoxicity and cardiac dysfunction in mammals and *Drosophila*. *Crit. Rev. Biochem. Mol. Biol.* **46**: 376–385.
11. Virtue, S., and A. Vidal-Puig. 2010. Adipose tissue expandability, lipotoxicity and the metabolic syndrome—an allostatic perspective. *Biochim. Biophys. Acta.* **1801**: 338–349.
12. Palanker Musselman, L., J. L. Fink, and T. J. Baranski. 2016. CoA protects against the deleterious effects of caloric overload in *Drosophila*. *J. Lipid Res.* **57**: 380–387.
13. Tennessen, J. M., W. E. Barry, J. Cox, and C. S. Thummel. 2014. Methods for studying metabolism in *Drosophila*. *Methods.* **68**: 105–115.
14. Laye, M. J., V. Tran, D. P. Jones, P. Kapahi, and D. E. L. Promislow. 2015. The effects of age and dietary restriction on the tissue-specific metabolome of *Drosophila*. *Aging Cell.* **14**: 797–808.
15. Reed, L. K., K. Lee, Z. Zhang, L. Rashid, A. Poe, B. Hsieh, N. Deighton, N. Glassbrook, R. Bodmer, and G. Gibson. 2014. Systems genomics of metabolic phenotypes in wild-type *Drosophila melanogaster*. *Genetics.* **197**: 781–793.
16. Williams, S., K. Dew-Budd, K. Davis, J. Anderson, R. Bishop, K. Freeman, D. Davis, K. Bray, L. Perkins, J. Hubickey, et al. 2015. Metabolomic and gene expression profiles exhibit modular genetic and dietary structure linking metabolic syndrome phenotypes in *Drosophila*. *G3 (Bethesda).* **5**: 2817–2829.
17. Xu, Y.-J., F. Luo, Q. Gao, Y. Shang, and C. Wang. 2015. Metabolomics reveals insect metabolic responses associated with fungal infection. *Anal. Bioanal. Chem.* **407**: 4815–4821.
18. Melo, C. F., D. N. de Oliveira, E. O. Lima, T. M. Guerreiro, C. Z. Esteves, R. M. Beck, M. A. Padilla, G. P. Milanez, C. W. Arns, J. L. Proença-Modena, et al. 2016. A lipidomics approach in the characterization of Zika-infected mosquito cells: potential targets for breaking the transmission cycle. *PLoS One.* **11**: e0164377.
19. Molloy, J. C., U. Sommer, M. R. Viant, and S. P. Sinkins. 2016. Wolbachia Modulates Lipid Metabolism in *Aedes albopictus* Mosquito Cells. *Appl. Environ. Microbiol.* **82**: 3109–3120.
20. Cázarez-García, D., M. Ramírez Loustalot-Laclette, T. Ann Markow, and R. Winkler. 2017. Lipidomic profiles of *Drosophila melanogaster* and cactophilic fly species: models of human metabolic diseases. *Integr. Biol. (Camb.)* **9**: 885–891.
21. Tortoriello, G., B. P. Rhodes, S. M. Takacs, J. M. Stuart, A. Basnet, S. Raboune, T. S. Widlanski, P. Doherty, T. Harkany, and H. B.

- Bradshaw. 2013. Targeted lipidomics in *Drosophila melanogaster* identifies novel 2-monoacylglycerols and N-acyl amides. *PLoS One*. **8**: e67865.
22. Chintapalli, V. R., M. Al Bratty, D. Korzekwa, D. G. Watson, and J. A. T. Dow. 2013. Mapping an atlas of tissue-specific *Drosophila melanogaster* metabolomes by high resolution mass spectrometry. *PLoS One*. **8**: e78066.
 23. Murphy, R. C., J. A. Hankin, and R. M. Barkley. 2009. Imaging of lipid species by MALDI mass spectrometry. *J. Lipid Res.* **50**: S317–S322.
 24. Vrkoslav, V., A. Muck, J. Cvačka, and A. Svatoš. 2010. MALDI imaging of neutral cuticular lipids in insects and plants. *J. Am. Soc. Mass Spectrom.* **21**: 220–231.
 25. Kaftan, F., V. Vrkoslav, P. Kynast, P. Kulkarni, S. Böcker, J. Cvačka, M. Knaden, and A. Svatoš. 2014. Mass spectrometry imaging of surface lipids on intact *Drosophila melanogaster* flies: intact bodies mass spectrometry imaging. *J. Mass Spectrom.* **49**: 223–232.
 26. Angel, P. M., J. M. Spraggins, H. S. Baldwin, and R. Caprioli. 2012. Enhanced sensitivity for high spatial resolution lipid analysis by negative ion mode matrix assisted laser desorption ionization imaging mass spectrometry. *Anal. Chem.* **84**: 1557–1564.
 27. Menger, R., C. Clendinen, L. Searcy, A. Edison, and R. Yost. 2015. MALDI mass spectrometric imaging of the nematode *Caenorhabditis elegans*. *Curr. Metabolomics*. **3**: 130–137.
 28. Khalil, S. M., J. Pretzel, K. Becker, and B. Spengler. 2017. High-resolution AP-SMALDI mass spectrometry imaging of *Drosophila melanogaster*. *Int. J. Mass Spectrom.* **416**: doi:10.1016/j.ijms.2017.04.001.
 29. Phan, N. T. N., A. S. Mohammadi, M. Dowlatshahi Pour, and A. G. Ewing. 2016. Laser desorption ionization mass spectrometry imaging of *Drosophila* brain using matrix sublimation versus modification with nanoparticles. *Anal. Chem.* **88**: 1734–1741.
 30. Phan, N. T. N., J. S. Fletcher, P. Sjövall, and A. G. Ewing. 2014. ToF-SIMS imaging of lipids and lipid related compounds in *Drosophila* brain: SIMS imaging of lipids, lipid related compounds in *Drosophila* brain. *Surf. Interface Anal.* **46**: 123–126.
 31. Krupp, J. J., and J. D. Levine. 2010. Dissection of oenocytes from adult *Drosophila melanogaster*. *J. Vis. Exp.* **41**: 2242.
 32. Lung, O., and M. F. Wolfner. 1999. *Drosophila* seminal fluid proteins enter the circulatory system of the mated female fly by crossing the posterior vaginal wall. *Insect Biochem. Mol. Biol.* **29**: 1043–1052.
 33. Folch, J., M. Lees, and G. H. Sloane Stanley. 1957. A simple method for the isolation and purification of total lipides from animal tissues. *J. Biol. Chem.* **226**: 497–509.
 34. Ulmer, C. Z., R. E. Patterson, J. P. Koelmel, T. J. Garrett, and R. A. Yost. 2017. A robust lipidomics workflow for mammalian cells, plasma, and tissue using liquid-chromatography high-resolution tandem mass spectrometry. *Methods Mol. Biol.* **1609**: 91–106.
 35. Koelmel, J. P., N. M. Kroeger, C. Z. Ulmer, J. A. Bowden, R. E. Patterson, J. A. Cochran, C. W. W. Beecher, T. J. Garrett, and R. A. Yost. 2017. LipidMatch: an automated workflow for rule-based lipid identification using untargeted high-resolution tandem mass spectrometry data. *BMC Bioinformatics*. **18**: 331.
 36. Patterson, R. E., A. S. Kirpich, J. P. Koelmel, S. Kalavalapalli, A. M. Morse, K. Cusi, N. E. Sunny, L. M. McIntyre, T. J. Garrett, and R. A. Yost. 2017. Improved experimental data processing for UHPLC-HRMS/MS lipidomics applied to nonalcoholic fatty liver disease. *Metabolomics*. **13**: doi:10.1007/s11306-017-1280-1.
 37. Xia, J., and D. S. Wishart. 2016. Using MetaboAnalyst 3.0 for comprehensive metabolomics data analysis. *Curr. Protoc. Bioinformatics*. **55**: 14.10.1–14.10.91.
 38. Chambers, M. C., B. Maclean, R. Burke, D. Amodei, D. L. Ruderman, S. Neumann, L. Gatto, B. Fischer, B. Pratt, J. Egerton, et al. 2012. A cross-platform toolkit for mass spectrometry and proteomics. *Nat. Biotechnol.* **30**: 918–920.
 39. Palm, W., J. L. Sampaio, M. Brankatschk, M. Carvalho, A. Mahmoud, A. Shevchenko, and S. Eaton. 2012. Lipoproteins in *Drosophila melanogaster*—assembly, function, and influence on tissue lipid composition. *PLoS Genet.* **8**: e1002828.
 40. Mousa, A., N. Naderpoor, N. Mellett, K. Wilson, M. Plebanski, P. J. Meikle, and B. de Courten. 2019. Lipidomic profiling reveals early-stage metabolic dysfunction in overweight or obese humans. *Biochim. Biophys. Acta Mol. Cell Biol. Lipids*. **1864**: 335–343.
 41. Razquin, C., E. Toledo, C. B. Clish, M. Ruiz-Canela, C. Dennis, D. Corella, C. Papanicolaou, E. Ros, R. Estruch, M. Guasch-Ferré, et al. 2018. Plasma lipidomic profiling and risk of type 2 diabetes in the PREDIMED Trial. *Diabetes Care*. **41**: 2617–2624.
 42. Kühnlein, R. P. 2012. Lipid droplet-based storage fat metabolism in *Drosophila*. *J. Lipid Res.* **53**: 1430–1436.
 43. Sultana, H., K. Miyazawa, S. Kanda, and H. Itabashi. 2011. Fatty acid composition of ruminal bacteria and protozoa, and effect of defaunation on fatty acid profile in the rumen with special reference to conjugated linoleic acid in cattle. *Anim. Sci. J.* **82**: 434–440.
 44. Zhang, X., Q. Jin, and L. H. Jin. 2017. High sugar diet disrupts gut homeostasis through JNK and STAT pathways in *Drosophila*. *Biochem. Biophys. Res. Commun.* **487**: 910–916.
 45. Pereira, M. T., M. Malik, J. A. Nostro, G. J. Mahler, and L. P. Musselman. 2018. Effect of dietary additives on intestinal permeability in both *Drosophila* and a human cell co-culture. *Dis. Model. Mech.* **11**: dmm034520.
 46. Scheitz, C. J. F., Y. Guo, A. M. Early, L. G. Harshman, and A. G. Clark. 2013. Heritability and inter-population differences in lipid profiles of *Drosophila melanogaster*. *PLoS One*. **8**: e72726.
 47. Wong, A. C-N., A. J. Dobson, and A. E. Douglas. 2014. Gut microbiota dictates the metabolic response of *Drosophila* to diet. *J. Exp. Biol.* **217**: 1894–1901.
 48. Unger, R. H., and P. E. Scherer. 2010. Gluttony, sloth and the metabolic syndrome: a roadmap to lipotoxicity. *Trends Endocrinol. Metab.* **21**: 345–352.
 49. Sletten, A. C., L. R. Peterson, and J. E. Schaffer. 2018. Manifestations and mechanisms of myocardial lipotoxicity in obesity. *J. Intern. Med.* **284**: 478–491.
 50. Dyntar D., M. Eppenberger-Eberhardt, K. Maedler, M. Pruschy, H. M. Eppenberger, G. A. Spinass, and M. Y. Donath. 2001. Glucose and palmitic acid induce degeneration of myofibrils and modulate apoptosis in rat adult cardiomyocytes. *Diabetes*. **50**: 2105–2113.
 51. Egnatchik, R. A., A. K. Leamy, S. A. Sacco, Y. E. Cheah, M. Shiota, and J. D. Young. 2019. Glutamate-oxaloacetate transaminase activity promotes palmitate lipotoxicity in rat hepatocytes by enhancing anaplerosis and citric acid cycle flux. *J. Biol. Chem.* **294**: 3081–3090.
 52. Liu, L., X. Shi, K. G. Bharadwaj, S. Ikeda, H. Yamashita, H. Yagyu, J. E. Schaffer, Y-H. Yu, and I. J. Goldberg. 2009. DGAT1 expression increases heart triglyceride content but ameliorates lipotoxicity. *J. Biol. Chem.* **284**: 36312–36323.
 53. Bosma, M., D. H. Dapito, Z. Drosatos-Tampakaki, N. Huipingson, L-S. Huang, S. Kersten, K. Drosatos, and I. J. Goldberg. 2014. Sequestration of fatty acids in triglycerides prevents endoplasmic reticulum stress in an in vitro model of cardiomyocyte lipotoxicity. *Biochim. Biophys. Acta*. **1841**: 1648–1655.
 54. Piccolis, M., L. M. Bond, M. Kampmann, P. Pulimeno, C. Chitruju, C. B. K. Jayson, L. P. Vaites, S. Boland, Z. W. Lai, K. R. Gabriel, et al. 2019. Probing the global cellular responses to lipotoxicity caused by saturated fatty acids. *Mol. Cell*. **74**: 32–44.e8.
 55. Drosatos, K., K. G. Bharadwaj, A. Lymperopoulos, S. Ikeda, R. Khan, Y. Hu, R. Agarwal, S. Yu, H. Jiang, S. F. Steinberg, et al. 2011. Cardiomyocyte lipids impair β -adrenergic receptor function via PKC activation. *Am. J. Physiol. Endocrinol. Metab.* **300**: E489–E499.
 56. Luukkonen, P. K., S. Sädevirta, Y. Zhou, B. Kayser, A. Ali, L. Ahonen, S. Lallukka, V. Pelloux, M. Gaggini, C. Jian, et al. 2018. Saturated fat is more metabolically harmful for the human liver than unsaturated fat or simple sugars. *Diabetes Care*. **41**: 1732–1739.
 57. Mente, A., M. Dehghan, S. Rangarajan, M. McQueen, G. Dagenais, A. Wielgosz, S. Lear, W. Li, H. Chen, S. Yi, et al. 2017. Association of dietary nutrients with blood lipids and blood pressure in 18 countries: a cross-sectional analysis from the PUREstudy. *Lancet Diabetes Endocrinol.* **5**: 774–787.
 58. Chaurasia, B., V. A. Kaddai, G. I. Lancaster, D. C. Henstridge, S. Sriram, D. L. A. Galam, V. Gopalan, K. N. B. Prakash, S. S. Velan, S. Bulchand, et al. 2016. Adipocyte ceramides regulate subcutaneous adipose browning, inflammation, and metabolism. *Cell Metab.* **24**: 820–834.
 59. Park, M., V. Kaddai, J. Ching, K. T. Fridianto, R. J. Sieli, S. Sugii, and S. A. Summers. 2016. A role for ceramides, but not sphingomyelins, as antagonists of insulin signaling and mitochondrial metabolism in C2C12 myotubes. *J. Biol. Chem.* **291**: 23978–23988.
 60. Chaurasia, B., T. S. Tippetts, R. Mayoral Monibas, J. Liu, Y. Li, L. Wang, J. L. Wilkerson, C. R. Sweeney, R. F. Pereira, D. H. Sumida, et al. 2019. Targeting a ceramide double bond improves insulin resistance and hepatic steatosis. *Science*. **365**: 386–392.
 61. Walls, S. M., A. Cammarato, D. A. Chatfield, K. Ocorr, G. L. Harris, and R. Bodmer. 2018. Ceramide-protein interactions modulate ceramide-associated lipotoxic cardiomyopathy. *Cell Reports*. **22**: 2702–2715.

62. Bandet, C. L., R. Mahfouz, J. Véret, A. Sotiropoulos, M. Poirier, P. Giussani, M. Campana, E. Philippe, A. Blachnio-Zabielska, R. Ballaire, et al. 2018. Ceramide transporter CERT is involved in muscle insulin signaling defects under lipotoxic conditions. *Diabetes*. **67**: 1258–1271.
63. Kang, S-J., S. P. Lall, and R. G. Ackman. 1997. Digestion of the 1-O-alkyl diacylglycerol ethers of Atlantic dogfish liver oils by Atlantic salmon *Salmo salar*. *Lipids*. **32**: 19–30.
64. Wallner, S., and G. Schmitz. 2011. Plasmalogens the neglected regulatory and scavenging lipid species. *Chem. Phys. Lipids*. **164**: 573–589.
65. Brites, P., H. R. Waterham, and R. J. A. Wanders. 2004. Functions and biosynthesis of plasmalogens in health and disease. *Biochim. Biophys. Acta*. **1636**: 219–231.
66. Wanders, R. J. A., and H. R. Waterham. 2006. Peroxisomal disorders: The single peroxisomal enzyme deficiencies. *Biochim. Biophys. Acta*. **1763**: 1707–1720.
67. Lodhi, I. J., X. Wei, L. Yin, C. Feng, S. Adak, G. Abou-Ezzi, F-F. Hsu, D. C. Link, and C. F. Semenkovich. 2015. Peroxisomal lipid synthesis regulates inflammation by sustaining neutrophil membrane phospholipid composition and viability. *Cell Metab*. **21**: 51–64.
68. Medina-Gomez, G., S. L. Gray, L. Yetukuri, K. Shimomura, S. Virtue, M. Campbell, R. K. Curtis, M. Jimenez-Linan, M. Blount, G. S. H. Yeo, et al. 2007. PPAR gamma 2 prevents lipotoxicity by controlling adipose tissue expandability and peripheral lipid metabolism. *PLoS Genet*. **3**: e64.
69. Colas, R., A. Sassolas, M. Guichardant, C. Cugnet-Anceau, M. Moret, P. Moulin, M. Lagarde, and C. Calzada. 2011. LDL from obese patients with the metabolic syndrome show increased lipid peroxidation and activate platelets. *Diabetologia*. **54**: 2931–2940.
70. Donovan, E. L., S. M. Pettine, M. S. Hickey, K. L. Hamilton, and B. F. Miller. 2013. Lipidomic analysis of human plasma reveals ether-linked lipids that are elevated in morbidly obese humans compared to lean. *Diabetol. Metab. Syndr*. **5**: 24.
71. Lodhi, I. J., L. Yin, A. P. L. Jensen-Urstad, K. Funai, T. Coleman, J. H. Baird, M. K. El Ramahi, B. Razani, H. Song, F. Fu-Hsu, et al. 2012. Inhibiting adipose tissue lipogenesis reprograms thermogenesis and PPAR γ activation to decrease diet-induced obesity. *Cell Metab*. **16**: 189–201.
72. Ando, A., M. Oka, and Y. Satomi. 2019. Deoxysphingolipids and ether-linked diacylglycerols accumulate in the tissues of aged mice. *Cell Biosci*. **9**: 61.
73. Samuel, V. T., Z-X. Liu, X. Qu, B. D. Elder, S. Bilz, D. Befroy, A. J. Romanelli, and G. I. Shulman. 2004. Mechanism of hepatic insulin resistance in non-alcoholic fatty liver disease. *J. Biol. Chem*. **279**: 32345–32353.
74. Barber, M. N., S. Risis, C. Yang, P. J. Meikle, M. Staples, M. A. Febbraio, and C. R. Bruce. 2012. Plasma lysophosphatidylcholine levels are reduced in obesity and type 2 diabetes. *PLoS One*. **7**: e41456.
75. Niehoff, A-C., H. Kettling, A. Pirkl, Y. N. Chiang, K. Dreisewerd, and J. Y. Yew. 2014. Analysis of *Drosophila* lipids by matrix-assisted laser desorption/ionization mass spectrometric imaging. *Anal. Chem*. **86**: 11086–11092.
76. Carvalho, M., J. L. Sampaio, W. Palm, M. Brankatschk, S. Eaton, and A. Shevchenko. 2012. Effects of diet and development on the *Drosophila* lipidome. *Mol. Syst. Biol*. **8**: 600.
77. Subramanian, M., S. K. Metya, S. Sadaf, S. Kumar, D. Schwudke, and G. Hasan. 2013. Altered lipid homeostasis in *Drosophila* InsP3 receptor mutants leads to obesity and hyperphagia. *Dis. Model. Mech*. **6**: 734–744.
78. Menger, R. F., W. L. Stutts, D. S. Anbukumar, J. A. Bowden, D. A. Ford, and R. A. Yost. 2012. MALDI mass spectrometric imaging of cardiac tissue following myocardial infarction in a rat coronary artery ligation model. *Anal. Chem*. **84**: 1117–1125.